Yuxi Li, Peter A. Hegarty, Michael Rüsing et al.

Ba(BO2OH) – A Monoprotonated Monoborate from Hydroflux Showing Intense Second Harmonic Generation

Erstveröffentlichung in / First published in:

Zeitschrift für anorganische und allgemeine Chemie. 2022. 648(21). Wiley. ISSN: 1521-3749.

DOI: https://doi.org/10.1002/zaac.202200193

Journal of Inorganic and General Chemistry
ZAAC
Zeitschrift für anorganische und allgemeine Chemie
www.zaac.wiley-vch.de
RESEARCH ARTICLE
Check for updates
DOI: 10.1002/zaac.202200193

$Ba(BO_2OH)$ – A Monoprotonated Monoborate from Hydroflux Showing Intense Second Harmonic Generation

Yuxi Li,[a] Peter A. Hegarty,[b] Michael Rüsing,[b] Lukas M. Eng,[b, c] and Michael Ruck*[a, c, d]

Dedicated to Professor Wolfgang Schnick on the Occasion of his 65th Birthday.

Pure samples of colorless, air-stable $Ba(BO_2OH)$ crystals were obtained from $Ba(NO_3)_2$ and H_3BO_3 under the ultra-alkaline conditions of a KOH hydroflux at about 250 °C. The product formation depends on the water-base molar ratio and the molar ratio of the starting materials. $B(OH)_3$ acts as a proton donor (Brønsted acid) rather than a hydroxide acceptor (Lewis acid). $Ba(BO_2OH)$ crystallizes in the non-centrosymmetric orthorhombic space group $P2_12_12_1$. Hydrogen bonds connect the almost planar $(BO_2OH)^{2-}$ anions, which are isostructural to HCO_3^-, into a syndiotactic chain. IR and Raman spectroscopy confirm the presence of hydroxide groups, which are involved in weak hydrogen bonds. Upon heating in air to about 450 °C, $Ba(BO_2OH)$ dehydrates to $Ba_2B_2O_5$. Moreover, the non-centrosymmetric structure of $Ba(BO_2OH)$ crystals was verified with power-dependent confocal Second Harmonic Generation (SHG) microscopy indicating large conversion efficiencies in ambient atmosphere.

Introduction

The significance of borates especially in optical applications has been emphasized in many papers and reviews.[1] In particular, metal borates,[2,3] e.g. β-BaB_2O_4 (BBO)[4], LiB_3O_5 (LBO)[5] or $KBe_2BO_3F_2$ (KBBF),[6] have been widely studied due to their diverse structures and nonlinear optical (NLO) properties such as second harmonic generation (SHG). In most cases, borates are obtained either by high temperature processes or under hydrothermal conditions. For example, the important nonlinear optical material β-BaB_2O_4 is typically grown from high temperature melts,[7] but is also available via hydrothermal synthesis in form of small particles[8] or accessible as thin films via sol-gel synthesis, pulsed laser deposition, opposed-targets magnetron sputtering, or metal-organic chemical vapor deposition.[9] Extreme high-pressure high-temperature conditions allow to synthesize uncommon borates, such as β-BaB_4O_7.[10]

We are currently exploring the potential of syntheses in hydroflux, an ultra-alkaline aqueous medium.[11] For a hydroflux, hydroxides of alkali metal or alkaline earth metals are combined with water in typical molar ratios of 1 to 2, corresponding to 50 or 25 molar (M) solutions. The hydroflux differs from hydrothermal conditions by the very low activity of water, so that syntheses are almost pressureless at about 200 °C. Hydroflux syntheses proceed within a few hours and require only a PTFE-lined autoclave that is inert to the alkaline medium and ensures that no water is lost during the reaction.

Using this approach, we were able to synthesize crystalline products of numerous oxo- and hydroxometalates.[12] Among them are cation conductors, while others can be used as carbon-free precursors to functional oxides. However, the method is by no means limited to these compound classes. An outlook on the possible applications of the hydroflux is given by the successful syntheses of the oxide iodide Ti_3OI,[13] the periodato complex $K_8[Rh(IO_6)_2]OH \cdot 3H_2O$,[14] the orthoselenate(IV) K_2SeO_3,[15] the tetraselenodiarsenate(II) $K_4(As_2Se_4) \cdot 2H_2O$,[16] and trichalcogenides such as K_2Te_3.[17] Remarkably, several of these products are sensitive to moisture but crystallize from an aqueous medium, which demonstrates another aspect of the low chemical activity of water in the hydroflux.

Here we report the first results of our research on the chemistry of borates in KOH hydroflux. The new monoprotonated monoborate $Ba(BO_2OH)$ isolated in this study was characterized structurally, in its thermal behavior and with respect to its nonlinear optical properties.

[a] Y. Li, Prof. Dr. M. Ruck
Faculty of Chemistry and Food Chemistry
Technische Universität Dresden
01062 Dresden, Germany
E-mail: michael.ruck@tu-dresden.de
[b] P. A. Hegarty, Dr. M. Rüsing, Prof. Dr. L. M. Eng
Institute of Applied Physics
Technische Universität Dresden
01187 Dresden, Germany
[c] Prof. Dr. L. M. Eng, Prof. Dr. M. Ruck
ct.qmat: Dresden-Würzburg Cluster of Excellence
Technische Universität Dresden
01062 Dresden, Germany
[d] Prof. Dr. M. Ruck
Max Planck Institute for Chemical Physics of Solids
Nöthnitzer Straße 40
01187 Dresden, Germany

Supporting information for this article is available on the WWW under https://doi.org/10.1002/zaac.202200193

Results and Discussion

Synthesis

In a first experiment on the chemistry of boric acid in such ultra-alkaline media and with the aim of preparing luminescent borate materials, we reacted $CeCl_3$ with $Ba(NO_3)_2$ and H_3BO_3 in a 40 M KOH hydroflux ($q(K) = n(H_2O):n(KOH) = 1.4$) for 10 h at 250 °C. The result were colorless crystals (Figure 1), which dissolve readily in water but are apparently insensitive to air. A crystal stored for four weeks under ambient conditions showed no signs of decomposition (Figure S1). An analysis with energy-dispersive X-ray spectroscopy (EDX) indicated the presence of barium and oxygen in the compound, but no cerium (the detector is not sensitive to boron). X-ray diffraction on a single-crystal revealed the composition $Ba(BO_2OH)$. Therefore, in a subsequent synthesis, $CeCl_3$ was omitted, but this led to the formation of $Ba_3(BO_3)_2$.[18]

Orthoboric acid is known to be a hydroxide acceptor (Lewis acid) rather than a proton donor (Brønsted acid). Under the ultra-alkaline conditions of hydroflux, however, $B(OH)_3$ is deprotonated to $(BO_2OH)^{2-}$ and $(BO_3)^{3-}$ despite the high availability of hydroxide ions (Equation 1).[19] Obviously, the driving force to obtain protons for the formation of water as well as the generation of additional hydrogen bonds in the hydroflux dominates. Auxiliary cations, such as cerium (Ce^{3+} as well as Ce^{4+}, tested with CeO_2), can replace the protons, bind hydroxide ions, and thus reduce the basicity of the hydroflux.

$$Ba(NO_3)_2 + B(OH)_3 + 2\ KOH \rightarrow Ba(BO_2OH) + 2\ KNO_3 + 2H_2O \quad (1)$$

Following these considerations, we modeled the decrease in basicity by decreasing the KOH concentration. As in many other cases, the base concentration $q(K)$ of the hydroflux turned out to be an important factor in the synthesis of $Ba(BO_2OH)$. Here, however, this also applies to the molar ratio $q(B) = n(B(OH)_3):n(Ba(NO_3)_2$. Unfortunately, $q(B)$ and $q(K)$ are not independent parameters due to the acid-base equilibria between $B(OH)_3$ and KOH.

Using the stoichiometric ratio of the starting materials, i.e. $q(B) = 1$, yielded little of the target compound and many by-products. Using a high excess of boric acid improved the yield and purity of $Ba(BO_2OH)$. Therefore, we chose the molar ratio $q(B) = 10$ for testing the influence of the base concentration $q(K)$. The different $q(K)$ and $q(B)$ ratios used are listed in Table S1.

Variation of $q(K)$ resulted in different products. Since we filled the autoclave in air and did not pretreat the solid KOH used, the reaction mixture always contained carbonate. In aqueous solution, this inevitably leads to precipitation of $BaCO_3$, but as we have found, this does not apply to ultra-alkaline media.

Using a comparatively water-rich hydroflux with $q(K) = 2.8$ resulted in the formation of $BaCO_3$ as the only solid product after washing with methanol (Figure S2a). For $q(K) < 2.8$, also $Ba(BO_2OH)$ forms. When q(K) was reduced to 1.85, the main product was $Ba(BO_2OH)$, but still needles of $BaCO_3$ were visible. Further increase of the base concentration to $q(K) = 1.4$ or 1.1 yielded cube-shaped colorless crystals of a yet unknown compound, but no or only traces of $BaCO_3$ or $Ba(BO_2OH)$.

We then kept the base concentration at $q(K) = 1.85$ and tested different ratios of $q(B)$ (Figure S2b). At $q(B) = 30$, no solid product was formed, presumably because the high boric acid content had lowered the pH of the solution too much. $Ba(BO_2OH)$ formed in the range of $10 \geq q(B) \geq 8$, but accompanied by impurities. Seemingly pure $Ba(BO_2OH)$ was obtained at $q(B) = 7$. In the range $6 \geq q(B) \geq 0.5$, $BaCO_3$ was formed as a by-product, increases more and more in its proportion and finally dominates the product.

Eventually, we used $q(K) = 1.85$ (30 M KOH) and $q(B) = 7$ as the optimum reaction conditions for the synthesis of $Ba(BO_2OH)$ and then removed the hydroflux and excess boric acid from the solid product by washing with methanol. After 10 h at 250 °C, a pure sample of $Ba(BO_2OH)$, according to the powder X-ray diffraction (PXRD) pattern (Figure 2), with a yield of about 90% (Ba based) was obtained.

Crystal Structure

The crystal structure of $Ba(BO_2OH)$ was initially solved and refined in the orthorhombic space group *Pnma*. The unit cell contains $Z = 4$ formula units. Despite very good *R* values, this

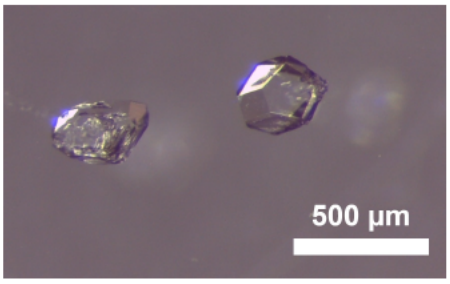

Figure 1. Photograph of representative $Ba(BO_2OH)$ crystals.

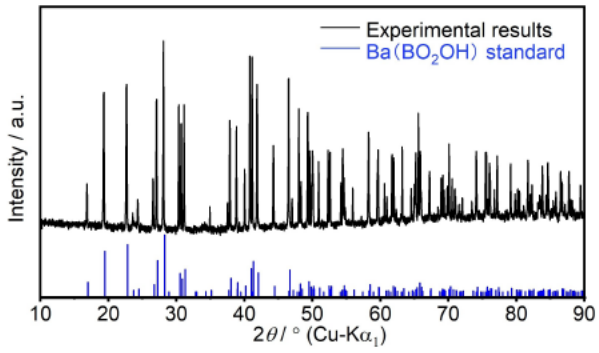

Figure 2. X-ray powder diffraction pattern ($CuK\alpha_1$ radiation) of a $Ba(BO_2OH)$ sample obtained with optimized synthesis parameters and the reference pattern simulated from single-crystal data.

Journal of Inorganic and General Chemistry
ZAAC
Zeitschrift für anorganische und allgemeine Chemie

solution was not satisfactory for two reasons. First, there was a long list of weak but significant reflections that violated both zonal reflection conditions. Second, the hydrogen atom was on a split position with 50% occupancy on both sides of the mirror plane and the O1 atom had a displacement ellipsoid elongated perpendicular to the mirror plane. Symmetry reduction to the maximal subgroup $P2_12_12_1$ resolved these issues (Figure 3). The axes were then exchanged according to increasing length: a = 586.68(6) pm, b = 729.01(7) pm, c = 751.65(8) pm. An inversion twin with almost equal twin volumes was identified. The hydrogen atom could be refined without restrictions. The atomic parameters are listed in Table S2 of the Supporting Information.

The $(BO_2OH)^{2-}$ anion is isoelectronic and isostructural to the HCO_3^- anion. The protonation of the O1 atom causes deviations of the $(BO_2OH)^{2-}$ anion from the trigonal-planar D_{3h} symmetry found for orthoboric acid $B(OH)_3$[20] and the $(BO_3)^{3-}$ anion, for example, in $Ca_3(BO_3)_2$.[21] As expected, the bond to the protonated O1 atom is longer than the other two (B–O1 144.2(2) pm, B–O2 134.3(5) pm, B–O3 134.8(5) pm) and the bond angles O–B–O deviate up to 6.2° from 120°. The hydrogen atom lies almost in the plane of the molecule and the angle B–O1–H is 109(3)°. The hydrogen atom is involved in a weak hydrogen bond O1–H···O1 with a donor-acceptor distance of 300 pm and an angle of 170.5°. These hydrogen bonds connect the $(BO_2OH)^{2-}$ anions into a syndiotactic chain that runs along the [100] direction (Figure S3).

The barium cation is eightfold coordinated through six closer, unprotonated oxygen atoms (Ba–O 269.2(2) to 282.6(2) pm) and two more distant, protonated ones (301.5(1) and 304.2(2) pm). The coordination polyhedron is a bicapped trigonal prism (Figure S4). Using the bond-length bond-strength correlation according to *Brese* and *O'Keeffe* the bond valence sum of the barium atom was calculated to 1.82 (R_{BaO} = 229 pm).[22]

$Ba(BO_2OH)$ is a new barium borate. The ICSD database lists numerous other ones, but all with higher water and/or B_2O_3 content. In 1958, *Lehmann* et al. reported $CaHBO_3$, which they had synthesized in six different ways, including several reactions under alkaline conditions. However, the structure was not determined.[23] Since then, the $(BO_2OH)^{2-}$ anion was found in few other synthetic compounds, such as $Na_2(BO_2OH)$,[24] $Sr(BO_2OH)$,[25] $Bi_2O_2(BO_2OH)$,[26] $Pb_2O(BO_2OH)$,[27] $[Pb_{18}O_{12}]Pb(BO_2OH)_2Cl_{10}$[28] and $Sr_5(BO_2OH)_3(OH)_3F$.[29] It is also a constituent of minerals such as sulfoborite, $Mg_3[SO_4(BO_2OH)_2]\cdot 4H_2O$,[30] szaibelyite, $Mg(BO_2OH)$,[31] sibirskite and parasibirskite, $Ca(BO_2OH)$.[32]

It seems that $Sr(BO_2OH)$ is isostructural to the barium compound. $Sr(BO_2OH)$ was described in the centrosymmetric space group *Pnma* with a = 699.1(2) pm, b = 570.7(2) pm and c = 695.2(3) pm.[25] The oxygen and the boron atoms on the mirror plane have elongated displacement ellipsoids (see above), while the hydrogen atom could not be localized. Presumably, the acentric space group $P2_12_12_1$ also applies to $Sr(BO_2OH)$. For $Ca(BO_2OH)$, two monoclinic polymorphs were described, sibirskite in the space group $P2_1/c$ (Z = 4) and parasibirskite in $P2_1/m$ (Z = 2).[32] $Mg(BO_2OH)$ crystallizes monoclinic in $P2_1/a$ (Z = 8).[31]

Infrared and Raman Spectra

For further characterization of the $(BO_2OH)^{2-}$ anion we measured infrared (IR) and Raman spectra of $Ba(BO_2OH)$ at room temperature. The anion is not trigonal symmetric because of the proton, but with respect to the vibrations it comes close to this symmetry because of the low mass of the proton.

The stretching vibration of the O–H group appears as weak broad band centered at 3428 cm^{-1} in the IR (Figure S5) and at 3427 cm^{-1} in the Raman spectrum (Figure 4). The comparatively high frequency correlates with the large O–H···O distance.[33] For comparison, in $Pb_2O(BO_2OH)$, the O–H vibration was detected at 3435 cm^{-1}.[27] For the assignment of signals at lower wavenumbers to vibrational modes of the borate anion, we refer to reports in literature.[27][34] The band around 1416 cm^{-1} (IR) and the weak resonance at 1367 cm^{-1} (Raman) can be assigned to the asymmetric B–O stretching mode in the borate anion. The symmetric stretching modes should be responsible for the

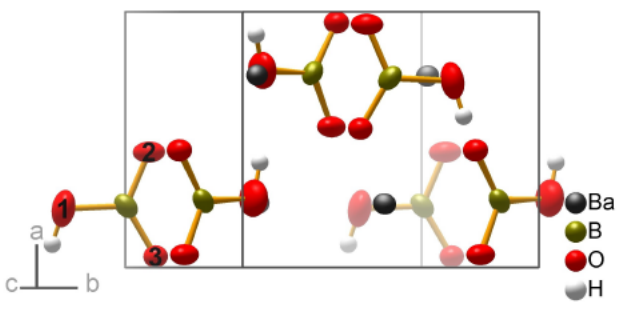

Figure 3. Crystal structure of $Ba(BO_2OH)$ with pseudo mirror planes perpendicular to the a-axis. Ellipsoids shown for the non-hydrogen atoms comprise 90% of the probability density.

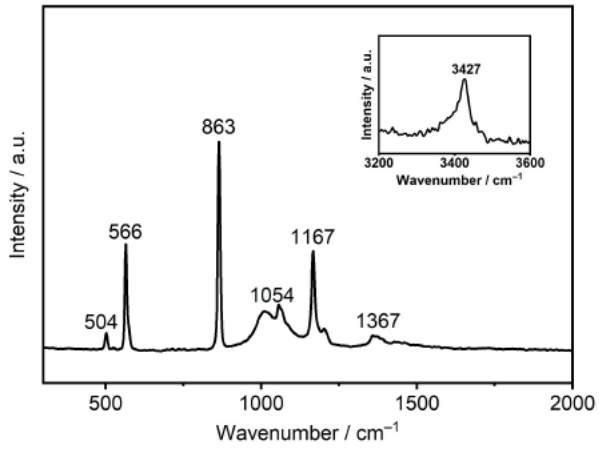

Figure 4. Raman spectrum of a single crystal of $Ba(BO_2OH)$ measured at room temperature.

weak absorption band at 1063 cm^{-1} (IR) and the group of signals at 1054 cm^{-1} (Raman). The bands observed at 1167 cm^{-1} (IR and Raman) can be assigned to the B–O–H bending mode.[35] The numerous signals between 900 and 500 cm^{-1} are attributed to the out-of-plane (at the higher wavenumbers) and in-plane bending modes of the borate group.[27,36] The bands at frequencies below 500 cm^{-1} are essentially due to lattice vibrations.[37]

Thermal Decomposition

A sample of $Ba(BO_2OH)$ was heated in a thermobalance under flowing argon. Weight loss began at about 250 °C, yet in several very small discrete steps, probably due to trace impurities or residuals of the hydroflux (Figure S6). The main weight loss occurred between 430 and 480 °C. The loss of 4.8 wt.–% corresponds to the evaporation of one water molecule per two formula units $Ba(BO_2OH)$ (calculated 4.6 wt.%). Repeating the experiment, but now in a stream of synthetic air, did not give significantly different results (Figure S7). To determine the product of the thermal treatment, a $Ba(BO_2OH)$ sample was annealed in air at 550 °C for 24 hours. The PXRD pattern revealed $Ba_2B_2O_5$ (Figure S8), which is the expected product of the dehydration process (Equation 2).

$$2\ Ba(BO_2OH) \rightarrow Ba_2B_2O_5 + H_2O \qquad (2)$$

Second Harmonic Generation (SHG)

Due to the non-centrosymmetric nature of the $Ba(BO_2OH)$ crystals, a second-harmonic (SH) optical response is expected. Figure 5 shows typical SH pictures recorded at the SH wavelength of 450 nm (blue light) for (a) the crossed and (b) the parallel alignment of polarizer and analyzer. Notably, all crystals excited at 900 nm (near IR) in the focal plane generate a strong response, with some crystals appearing even brighter when using parallel-polarized detection, while others show a similar overall response independent of polarization. Due to the powdered nature of the sample, the crystal orientation of the individual crystallites with respect to laser propagation direction and polarization is unknown and, therefore, it is not possible to extract information on the tensorial character of the SH signal. To unambiguously prove SH generation, we tested the power dependence of the SH signal that must scale quadratically as a function of incident power, i.e. $I_{SHG} \propto I^2_{pump}$.[38]

Figure 5c displays this power dependence as recorded in parallel polarization, clearly indicating the quadratic law for the two selected crystallites in Figure 5b. While these measurements demonstrate the second-order nonlinear response of the crystals, we cannot draw any definitive conclusions on the magnitude of individual SHG tensor elements yet due to the unknown influence of various factors. Such a study is beyond the scope of this present work and will require further knowledge of the material's refractive indices and dispersion,

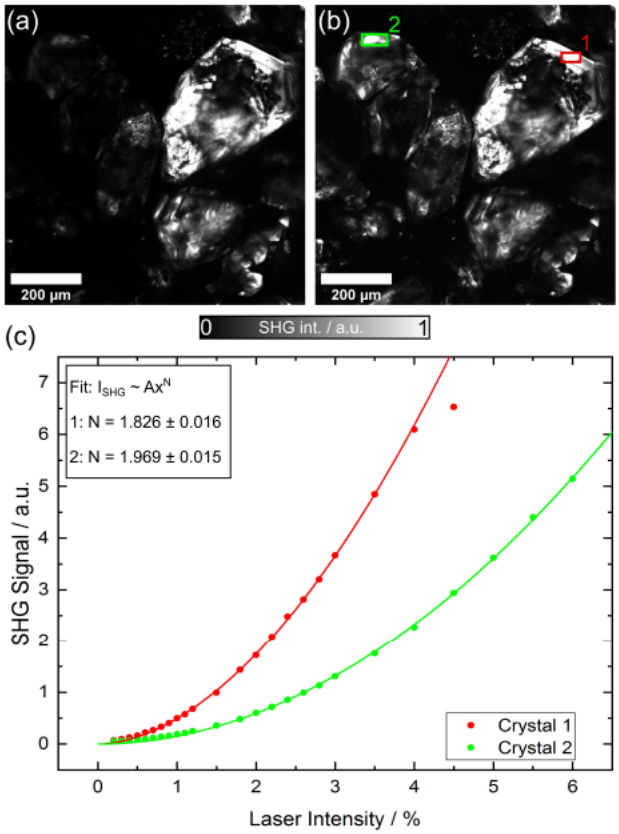

Figure 5. Second harmonic images of a selection of $Ba(BO_2OH)$ crystallites examined at a fundamental wavelength of 900 nm and an average fundamental power of 130 mW in (a) cross-polarization and (b) parallel polarization of pump and detected light, respectively. Parallel polarization reveals a slightly enhanced response for some selected crystallites, however, due to their unknown orientation within the powder, it is difficult to infer the participating tensor elements. (c) Power dependent response at 900 nm fundamental wavelength recorded in parallel polarization for the two $Ba(BO_2OH)$ crystallites marked in (b). Both show the expected quadratic behavior, though with a slightly different strength.

absorption coefficient, and a study of optical confinement in these µm-sized crystals,[39] as well as knowledge on their relative orientation.

Conclusions

In this work, the new barium borate $Ba(BO_2OH)$ was crystallized from a KOH hydroflux. The barium compound completes the series of alkaline earth salts with the almost planar $(BO_2OH)^{2-}$ anion. The synthesis is strongly influenced by acid-base equilibria involving $B(OH)_3$, H_2O, and OH^-. When optimizing the reaction conditions, it was therefore necessary to optimize not only the ratio of water to base, as is common in hydroflux syntheses, but also the ratio of boric acid to base. The crystallization of the $(BO_2OH)^{2-}$ anion reveals that $B(OH)_3$ acts as a proton donor (Brønsted acid) rather than a hydroxide accept-

or (Lewis acid) under ultra-alkaline conditions. If the base concentration is sufficiently high, the formation of the by-product $BaCO_3$ is suppressed. Thus, it was demonstrated for the first time that hydroflux is also suitable as an efficient synthetic route for borates.

The transparent $Ba(BO_2OH)$ crystals obtained in high yield after only 10 hours of reaction time were suitable for the determination of the crystal structure. The observation of an intense SHG effect confirmed that the structure is not centrosymmetric.

Experimental Section

Synthesis: $Ba(BO_2OH)$ was synthesized in a KOH hydroflux. The reaction was carried out in a PTFE-lined 50 mL Berghof type DAB-2 autoclave to prevent water loss. In the optimized synthesis protocol, starting from 0.86 mmol $Ba(NO_3)_2$ (≥99%, Sigma-Aldrich) and 6 mmol $B(OH)_3$ (99.99%, abcr), i.e. $q(B) = 7$, 3 mL (167 mmol) water and then 5.13 g (92 mmol) KOH (86%, Fisher Scientific), i.e. $q(K) = 1.85:1$, were added under ambient conditions. The autoclave was heated to 250 °C at 2 K min^{-1}, held for 10 h before cooling down to room temperature at a rate of −0.3 K min^{-1}. The reaction products were washed with methanol and the resulting $Ba(BO_2OH)$ was stored in air. For test with different $q(B)$ or $q(K)$, the amount of $Ba(NO_3)_2$ or KOH was changed (see also Table S2).

Crystal Structure Determination: Intensity data was collected at 100(1) K with a four-circle diffractometer Kappa Apex2 (Bruker) equipped with a CCD-detector using graphite-monochromated Mo-K_α radiation ($\lambda = 71.073$ pm). The raw data were corrected for background, Lorentz and polarization factors,[40] and multi-scan absorption correction was applied.[41] The structures were solved using intrinsic phasing in the ShelXT program.[42] Structure refinement against F_o^2 with ShelXL[43] included anisotropic displacement parameters for all non-hydrogen atoms. Graphical representations of the structures were developed with Diamond.[44]

$Ba(BO_2OH)$: orthorhombic; $P2_12_12_1$ (no. 19); $T = 100(1)$ K; $a = 586.68(6)$ pm, $b = 729.01(7)$ pm, $c = 751.65(8)$ pm, $V = 321.48(6)\cdot10^6$ pm^3; $Z = 4$; $\rho_{calc.} = 4.074$ g cm^{-3}; μ(Mo-K_α) = 12.1 mm^{-1}; $2\theta_{max} = 80.8°$, $-10 \le h \le 10$, $-13 \le k \le 13$, $-13 \le l \le 13$; 21094 measured, 2041 unique reflections, $R_{int} = 0.024$, $R_\sigma = 0.012$; 52 parameters; extinction parameter $262(9)\cdot10^{-4}$; inversion twin with volume ratio 0.54:0.46(4); $R_1[2024\ F_o > 4\sigma(F_o)] = 0.013$, wR_2(all F_o^2) = 0.022, $GooF = 1.85$; residual electron density: −1.23 to 0.78 e 10^{-6} pm^{-3}. Further details on the crystal structure investigation can be obtained from the Fachinformationszentrum Karlsruhe, 76344 Eggenstein-Leopoldshafen, Germany (fax: +49-7247-808-666; e-mail:crysdata@fiz-karlsruhe.de), or from the Cambridge Crystallographic Data Centre via www.ccdc.cam.ac.uk/structures, on quoting the depository number CSD-2176629.

SEM Analysis: Scanning electron microscopy (SEM) was performed using a SU8020 (Hitachi) with a triple detector system for secondary and low-energy backscattered electrons ($U_a = 5$ kV). The composition of selected single crystals was determined by semi-quantitative energy dispersive X-ray analysis ($U_a = 15$ kV) using a Silicon Drift Detector (SDD) X–Max^N (Oxford Instruments). The data were processed with the AZtec software package (Oxford Instruments, 2013).

Powder X-ray Diffraction: Powder samples were investigated at room temperature on a Stadi P (Stoe & Cie.) diffractomter equipped with a curved Ge-monochromator and a Dectris Mythen 1 K detector using Cu–Kα_1 radiation ($\lambda = 154.056$ pm).

Thermal Analysis: $Ba(BO_2OH)$ samples were heated to 600 °C at a rate of 5 K min^{-1}.under a dynamic flow of synthetic air (CO_2 free) or argon in a STA 409 C/CD (Netzsch).

IR Spectroscopy: IR spectra were recorded using a Bruker Vertex 70 FT-IR spectrometer. The device was operated in the ATR mode (diamond), working with a measuring range of 4000 to 500 cm^{-1}. Data analysis was performed with the program OPUS.

Raman Spectroscopy: The spectrum (100 scans) was recorded with a Bruker RFS 100 Fourier transform Raman spectrometer with a 1064 nm Nd-YAG-Laser with a laser power of 227 mW.

SHG: Crystallites of several 100 μm size were distributed on a microscopy glass slide and analyzed in a Zeiss LSM980 microscope with a linear polarized, femtosecond laser source (Spectra Physics Insight X3, 690–1300 nm, pulse duration < 100 s, up to 5 W) attached (details on the experimental setup can be found in previous work.[38] The fundamental light was focused through the microscopy glass slide on the crystals and the generated light was collected via the same objective lens in back reflection. The generated SH light was separated via appropriate filters (Schott BG39) and detected via the photomultiplier tube system of the microscope. The polarization of the generated SH light was analyzed with linear polarizers and detection was performed with parallel and in cross-polarization with respect to the pump light.

Acknowledgements

We thank Yiran Wang and Tobias Pietsch (both TU Dresden) for technical assistance with the SEM and the Raman spectrometer. This work was supported by the Light Microscopy Facility of TU Dresden. We express our gratitude for financial support by the Deutsche Forschungsgemeinschaft (ID: 438795198) and the Würzburg-Dresden Cluster of Excellence on "Complexity and Topology in Quantum Matter — ct.qmat" (EXC 2147; ID: 39085490). Yuxi Li was supported by the China Scholarship Council (CSC). Open Access funding enabled and organized by Projekt DEAL.

Conflict of Interest

The authors declare no conflict of interest.

Data Availability Statement

The data that support the findings of this study are available in the supplementary material of this article.

Keywords: borates · crystal structure · hydroflux · pseudosymmetry · SHG effect

[1] M. Mutailipu, K. R. Poeppelmeier, S. Pan, *Chem. Rev.* **2021**, *121*, 1130–1202.
[2] X. Fan, *Crit. Rev. Environ. Sci. Technol.* **2021**, *52*, 2227–2269.
[3] C. T. Chen, T. Sasaki, R. K. Li, Y. C. Wu, Z. S. Lin, Y. Mori, Z. G. Hu, J. Y. Wang, S. Uda, M. Yoshimura, Y. Kaneda, *Nonlinear optical*

borate crystals: Principals and applications, Wiley-VCH, Weinheim, **2012**, pp 15–246.
[4] C. T. Chen, B. Wu, A. D. Jiang, G. M. You, *Sci. Sin. B* **1985**, *28*, 235–243.
[5] C. T. Chen, Y. C. Wu, A. D. Jiang, B. C. Wu, G. M. You, R. K. Li, S. J. Lin, *J. Opt. Soc. Am. B* **1989**, *6*, 616–621.
[6] C. T. Chen, G. L. Wang, X. Y. Wang, Z. Y. Xu, *Appl. Phys. B: Lasers Opt.* **2009**, *97*, 9–25.
[7] P. P. Fedorov, A. E. Kokh, N. G. Kononova, *Russ. Chem. Rev.* **2002**, *71*, 651–671.
[8] J. Zhang, G. He, R. Li, X. Chen, *J. Alloys Compd.* **2009**, *489*, 504–508.
[9] J. Liu, H. Wang, X. He, G. Zhao, G. Zhou, J. Xu, *Guisuanyan Xuebao* **2004**, *32*, 636–641.
[10] J. S. Knyrim, S. R. Römer, W. Schnick, H. Huppertz, *Solid State Sci.* **2009**, *11*, 336–242.
[11] a) D. E. Bugaris, M. D. Smith, H.-C. zur Loye, *Inorg. Chem.* **2013**, *52*, 3836–3844; b) W. M. Chance, D. E. Bugaris, A. S. Sefat, H.-C. zur Loye, *Inorg. Chem.* **2013**, *52*, 11723–11733.
[12] a) R. Albrecht, J. Hunger, T. Block, R. Pöttgen, A. Senyshyn, T. Doert, M. Ruck, *ChemistryOpen* **2019**, *8*, 74–83; b) R. Albrecht, J. Hunger, T. Doert, M. Ruck, *Eur. J. Inorg. Chem.* **2019**, 1398–1405; c) R. Albrecht, J. Hunger, M. Hölzel, T. Block, R. Pöttgen, T. Doert, M. Ruck, *ChemistryOpen* **2019**, *8*, 1399–1406; d) R. Albrecht, J. Hunger, T. Doert, M. Ruck, *Z. Anorg. Allg. Chem.* **2020**, *646*, 1130–1137; e) R. Albrecht, T. Doert, M. Ruck, *Z. Anorg. Allg. Chem.* **2020**, *646*, 1389–1395; f) R. Albrecht, T. Doert, M. Ruck, *Z. Anorg. Allg. Chem.* **2020**, *646*, 1517–1524; g) R. Albrecht, F. Graßme, T. Doert, M. Ruck, *Z. Naturforsch. B* **2020**, *75*, 951–957; h) R. Albrecht, J. Hunger, M. Hölzel, E. Suard, W. Schnelle, T. Doert, M. Ruck, *Eur. J. Inorg. Chem.* **2021**, 364–376; i) R. Albrecht, H. Poddig, J. Hunger, M. Ruck, P. Benrath, A. Möller, T. Doert, *Z. Anorg. Allg. Chem.* **2021**, *647*, 667–672; j) R. Albrecht, V. Bretschneider, T. Doert, M. Ruck, *Z. Anorg. Allg. Chem.* **2021**, *647*, 1702–1708; k) R. Albrecht, M. Hoelzel, H. Beccard, M. Rüsing, L. M. Eng, T. Doert, M. Ruck, *Chem. Eur. J.* **2021**, *27*, 14299–14306; l) R. Albrecht, M. Ruck, *Z. Naturforsch. B* **2022**, *77*, DOI: 10.1515/znb-2022–0016.
[13] R. Albrecht, H. Menning, T. Doert, M. Ruck, *Acta Crystallogr. Sect. E* **2020**, *76*, 1638–1640.
[14] H. He, R. Albrecht, M. Ruck, *Z. Anorg. Allg. Chem.* **2022**, *648*, e202200041.
[15] R. Albrecht, T. Doert, M. Ruck, *Acta Crystallogr. Sect. E* **2022**, *78*, 615–618.
[16] R. Albrecht, F. Jach, M. Ruck, *Z. Anorg. Allg. Chem.* **2022**, *648*, e202100306.
[17] R. Albrecht, M. Ruck, *Angew. Chem.* **2021**, *133*, 22744–22752; *Angew. Chem. Int. Ed.* **2021**, *60*, 22570–22577.
[18] T. B. Bekker, S. V. Rashchenko, Y. V. Seryotkin, A. E. Kokh, A. V. Davydov, P. P. Fedorov, *J. Am. Ceram. Soc.* **2018**, *101*, 450–457.
[19] J. Yang, X. Pan, R. Quhe, K. Bi, S. Lin, C. Liang, C. Yao, Y. Du, J. Liu, D. Fan, H. Yang, Y. Wang, M. Lei, *Micro Nano Lett.* **2017**, *12*, 430–434.
[20] M. Gajhede, S. Larsen, S. Rettrup, *Acta Crystallogr. Sect. B* **1986**, *42*, 545–552.
[21] A. Vegas, F. H. Cano, S. Garcia Blanco, *Acta Crystallogr. Sect. B* **1975**, *31*, 1416–1419.
[22] N. E. Brese, M. O'Keeffe, *Acta Crystallogr. Sect. B* **1991**, *47*, 192–197.
[23] H.-A. Lehmann, A. Zielfelder, G. Herzog, *Z. Anorg. Allg. Chem.* **1958**, *296*, 199–207.
[24] S. Menchetti, C. Sabelli, *Acta Crystallogr. Sect. B* **1982**, *38*, 1282–1285.
[25] Z.-T. Yu, Z. Shi, W. Chen, Y.-S. Jiang, H.-M. Yuan, J.-S. Chen, *Dalton Trans.* **2002**, 2031–2035.
[26] R. Cong, J. Sun, T. Yang, M. Li, F. Liao, Y. Wang, J. Lin, *Inorg. Chem.* **2011**, *50*, 5098–5104.
[27] F. Sun, L. Wang, C. C. Stoumpos, *J. Solid State Chem.* **2016**, *240*, 61–66.
[28] O. I. Siidra, H. Kabbour, O. Mentre, E. V. Nazarchuk, P. Kegler, D. O. Zinyakhina, M. Colmont, W. Depmeier, *Inorg. Chem.* **2016**, *55*, 9077–9084.
[29] Y. Dong, L. Gao, Z. Su, *J. Mol. Struct.* **2021**, *1227*, 128915.
[30] O. Braitsch, *Beitr. Mineral. Petrogr.* **1961**, *8*, 60–66.
[31] J. D. Grice, *Can. Mineral.* **2008**, *46*, 671–677.
[32] W. Sun, Y.-X. Huang, Z. Li, Y. Pan, J.-X. Mi, *Can. Mineral.* **2011**, *49*, 823–834.
[33] B. K. Nakamoto, M. Margoshes, R. E. Rundle, *J. Am. Chem. Soc.* **1955**, *77*, 6480–6486.
[34] a) T. S. Ortner, K. Wurst, M. Seibald, B. Joachim, H. Huppertz, *Eur. J. Inorg. Chem.* **2016**, 3292–3298; b) Y. P. Biryukov, R. S. Bubnova, M. G. Krzhizhanovskaya, S. K. Filatov, A. V. Povolotskiy, V. L. Ugolkov, *Solid State Sci.* **2020**, *99*, 106061; c) Y. Wang, S. Pan, X. Hou, G. Liu, J. Wang, D. Jia, *Solid State Sci.* **2010**, *12*, 1726–1730; d) W. Zhu, X. Wang, X. Zhang, H. Zhang, Q. Zhang, *Cryst. Growth Des.* **2011**, *11*, 2935–2941; e) Li, Jun, Xia, Shuping, S. Gao, *Spectrochim. Acta* **1995**, *51 A*, 519–532; f) G. D. Chryssikos, J. A. Kapoutsis, A. P. Patsis, E. I. Kamitsos, *Spectrochim. Acta* **1991**, *47 A*, 1117–1126.
[35] a) W. Zhao, *J. Mol. Struct.* **2017**, 1127, 252–256; b) F. Spadaro, A. Rossi, S. N. Ramakrishna, E. Laine, P. Woodward, N. D. Spencer, *Langmuir* **2018**, *34*, 2219–2234.
[36] a) Q. Zhao, X. Zhu, X. Bai, H. Fan, Y. Xie, *Eur. J. Inorg. Chem.* **2007**, 1829–1834; b) G. D. Chryssikos, *J. Raman Spectrosc.* **1991**, *22*, 645–650.
[37] J. Andrieux, C. Goutaudier, L. Laversenne, E. Jeanneau, P. Miele, *Inorg. Chem.* **2010**, *49*, 4830–4835.
[38] a) F. Jach, F. R. Wagner, Z. H. Amber, M. Rüsing, J. Hunger, Y. Prots, M. Kaiser, M. Bobnar, A. Jesche, L. M. Eng, M. Ruck, P. Höhn, *Angew. Chem.* **2021**, *133*, 16015–16021; *Angew. Chem. Int. Ed.* **2021**, *60*, 15879–15885; b) D. Tan, B. Kirbus, M. Rusing, T. Pietsch, M. Ruck, L. M. Eng, *Small* **2020**, *16*, e2000857; c) D. Tan, B. Kirbus, L. M. Eng, M. Ruck, *Eur. J. Inorg. Chem.* **2020**, 2465–2469.
[39] Z. H. Amber, B. Kirbus, L. M. Eng, M. Rüsing, *J. Appl. Phys.* **2021**, *130*, 133102.
[40] *APEX2*, Bruker AXS Inc., Madison, Wisconsin, USA, **2014**.
[41] G. M. Sheldrick, *Sadabs, Area-Detector Absorption Correction*, Bruker AXS Inc., Madison, Wisconsin, USA, **2014**.
[42] G. M. Sheldrick, *ShelXT*, Universität Göttingen, Germany, **2014**.
[43] G. M. Sheldrick, *Acta Crystallogr. Sect. A* **2008**, *64*, 112–122.
[44] K. Brandenburg, *Diamond 4, Crystal and Molecular Structure Visualization*, Crystal Impact GbR, Bonn, Germany, **2017**.

Manuscript received: June 9, 2022
Revised manuscript received: July 14, 2022
Accepted manuscript online: July 20, 2022